

Nanoscale

Accepted Manuscript



This is an *Accepted Manuscript*, which has been through the Royal Society of Chemistry peer review process and has been accepted for publication.

Accepted Manuscripts are published online shortly after acceptance, before technical editing, formatting and proof reading. Using this free service, authors can make their results available to the community, in citable form, before we publish the edited article. We will replace this *Accepted Manuscript* with the edited and formatted *Advance Article* as soon as it is available.

You can find more information about *Accepted Manuscripts* in the [Information for Authors](#).

Please note that technical editing may introduce minor changes to the text and/or graphics, which may alter content. The journal's standard [Terms & Conditions](#) and the [Ethical guidelines](#) still apply. In no event shall the Royal Society of Chemistry be held responsible for any errors or omissions in this *Accepted Manuscript* or any consequences arising from the use of any information it contains.

Origin of the Luminescence from ZnO/CdS Core/shell Nanowire Arrays

Zhiqiang Wang^{1,3}, Jian Wang², Tsun-Kong Sham^{1,*} and Shaoguang Yang³

¹Department of Chemistry, the University of Western Ontario, London, Canada N6A 5B7

²Canadian Light Source Inc., University of Saskatchewan, Saskatoon, Canada S7N 2V3

³Nanjing National Laboratory of Microstructures and School of Physics, Nanjing University, Nanjing, China 210093

* Author to whom correspondence should be addressed. Email: tsham@uwo.ca

Prof. Tsun-Kong Sham

Department of Chemistry, The University of Western Ontario

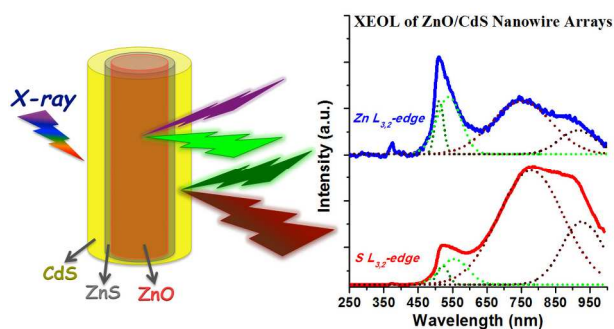
Chemistry Building, 1151 Richmond Street, London, Ontario, Canada N6A 5B7

Phone: (519) 661-2111 ext. 86341

Fax: (519) 661-3022

E-mail: tsham@uwo.ca

Table of Contents Graphic



KEYWORDS. Luminescence, nano-composites, XANES spectroscopy, STXM, spectro-microscopy.

Abstract:

Chemical imaging, electronic structure and optical properties of ZnO/CdS nano-composites have been investigated using scanning transmission X-ray microscopy (STXM), X-ray absorption near-edge structures (XANES) and X-ray excited optical luminescence (XEOL) spectroscopies. STXM and XANES results confirm that the as-prepared product is ZnO/CdS core/shell nanowires (NWs), and further indicate that ZnS was formed on the surface of ZnO NWs as the interface between ZnO and CdS. The XEOL from ZnO/CdS NW arrays exhibits one weak ultraviolet (UV) emission at 375 nm, one strong green emission at 512 nm, and two broad infrared (IR) emissions at 750 and 900 nm. Combining XANES and XEOL, it is concluded that the UV luminescence is the near band gap emission (BGE) of ZnO; the green luminescence comes from both the BGE of CdS and defect emission (DE, zinc vacancies) of ZnO; the IR luminescence is attributed to the DE (bulk defect related to S site) of CdS; ZnS contributes little to the luminescence of the ZnO/CdS NW arrays. Interestingly, the BGE and DE from oxygen vacancies of ZnO in the ZnO/CdS nano-composites are almost entirely quenched, while DE from zinc vacancies changes little.

KEYWORDS. Luminescence, nano-composites, XANES spectroscopy, STXM, spectro-microscopy.

Introduction

The peculiar physical and chemical properties of materials strongly depend on their morphology and size in nanoscale.¹ Luminescence is one of the most important methods for studying the electronic properties of nanostructures. For nano-composites, the luminescence can become quite complex due to the presence of multiple phases, interfaces and surfaces. Thus, it is a challenge to analyze the luminescence spectra of nano-composites, particularly when the components exhibit emissions in the same wavelength region of the spectrum (overlap of luminescence from each component).² Here we demonstrate how synchrotron-based elemental, site and excitation channel specific techniques such as X-ray excited optical luminescence (XEOL) and X-ray

absorption near edge structure (XANES) are utilized to understand the origin of luminescence from the ZnO/CdS core/shell nanowire (NW) arrays.

ZnO and CdS, important II-VI semiconductors with a direct band gap of 3.37 and 2.42 eV respectively, have prominent applications in electronic and optoelectronic devices.³⁻⁵ At room temperature, ZnO nanostructures often exhibit a sharp near band gap emission (BGE) in the ultraviolet (UV) region and a broad defect emission (DE) in the green region that is related to oxygen/zinc vacancies, and sometimes a broad surface defect peak in the red/infrared (IR) region.⁶⁻⁸ While CdS nanostructures with a smaller band gap energy always show green (near BGE) and IR (DE, cadmium or sulfur vacancies) luminescence.^{9, 10} In ZnO/CdS nano-composites, both ZnO and CdS can contribute to the green (DE of ZnO and near BGE of CdS) and red/IR (DE of ZnO and CdS) luminescence. It is also possible that the luminescence of one component is quenched by the other.^{11, 12} Due to the large lattice mismatch between ZnO and CdS, new defects can be created in the ZnO/CdS interface that will also lead to luminescence. Therefore, it is difficult to probe with conventional techniques the origin of luminescence in such ZnO/CdS nano-composites, which is important for their application in solar cells.¹³⁻¹⁵

Synchrotron-based spectroscopic techniques using a bright and widely energy tunable light source provide unique capabilities, such as site, element, excitation channel (absorption edge) and chemical specificity, in studying light emitting materials, especially luminescent nano-composites.^{11, 16-18} The techniques we used in this study include scanning transmission X-ray microscopy (STXM), X-ray absorption near edge structure (XANES) and X-ray excited optical luminescence (XEOL). STXM employs a nano-sized X-ray beam and provides spectromicroscopic information by measuring the absolute absorption of the specimen in transmission mode; thus both chemical images and detailed absorption spectroscopic features of a single nanostructure (including its thickness) can be revealed.¹⁹ XANES probes the local structure and bonding of the absorbing atom by monitoring the absorption coefficient at an absorption edge of interest, and can provide information on the oxidation state, coordination, and

symmetry of the system. XEOL, an X-ray-photon in/optical-photon out technique, has been shown to be a powerful tool for the investigation of the local chemical environment of a site that gives rise to a particular luminescence band. Recently, we have used XEOL to probe the origin of the luminescence from BN nanotubes and the nature of the optical luminescence from GaN-ZnO solid solution nanostructures.^{20, 21} In the present paper, STXM, XEOL and XANES measurements were carried out at different absorption edges to reveal the origin of different luminescence channels and the corresponding electronic structures in ZnO/CdS core/shell NW arrays.

EXPERIMENTAL DETAILS

Sample preparation. The synthesis of the ZnO/CdS core/shell NW arrays was carried out in a horizontal furnace via a two-step vapor-phase transport method. ZnO NW arrays were firstly prepared following a previously reported procedure.^{22, 23} Briefly, a mixture of ZnO (> 99.0 %, Tianjin Zhiyuan Chemical Reagent Co., Ltd.) and graphite (> 99.85 %, Shanghai Huayuan Fine Chemical Industry Co., Ltd.) powders was used as source materials. Si (100) wafer (Hangzhou Haina Semiconductor Co., Ltd.) was cleaned by ultrasound in acetone and ethanol, rinsed with dionized water and dried by N₂ flow. Then the Si wafer was coated with a layer of gold thin film (about 10 nm thick with settings of 25 mA, 40 mm, 60 seconds and 8×10^{-2} mbar) via K550X Sputter Coater (Quorum Technologies Ltd.) and used as the substrate placing above the source materials. The temperature of the furnace was raised to 850 °C and typically kept at that temperature for 60 minutes under a constant flow of argon (99.99%, 20 sccm). After the furnace was cooled to room temperature, a layer of gray powder was found on the surface of the Si wafer. In the following step, 0.2 g of CdS (99.99 %, Alfa Aesar) was placed in the center of a quartz tube. The Si wafer, already deposited with a layer of ZnO, was used as the substrate and placed downstream in the quartz tube, 8 cm away from the CdS powder. Prior to heating, the system was flushed with high-purity N₂ for 10 minutes to eliminate O₂ from the quartz tube. Then, the furnace was raised to 750 °C and kept at that temperature for 1 minute under a constant flow of nitrogen (40 sccm). After the furnace was cooled to room temperature, the colour of the Si wafer

surface changed from gray to yellow.

Characterization. The crystal structures and morphologies of the products were characterized by X-ray powder diffraction (XRD; Rigaku RU-200BVH) with Co K α radiation ($\lambda = 1.7892 \text{ \AA}$), scanning electron microscopy (SEM; Philips-XL30), and transmission electron microscopy (TEM; Philips CM 10), respectively. Photoluminescence (PL) spectra were recorded by Mightex spectrometer excited with the 406 nm laser.

Synchrotron measurements. STXM measurement was conducted at the SM beamline of the Canadian Light Source (CLS), which is equipped with a 25 nm outermost-zone zone plate (CXRO, Berkeley Lab). The diffraction-limited spatial resolution for this zone plate is 30 nm. A few mg of the sample was collected from the substrate and dispersed in methanol by brief sonication, then deposited on a Si₃N₄ window (thickness: 100 nm, Norcada Inc.) and allowed to dry in the air before transferred into the STXM chamber. Image sequence (stack) scans over a range of photon energies were acquired for the same sample region at Zn L_{3,2}-edge, O K-edge and S L_{3,2}-edge. STXM data were analyzed using the aXis2000 software package,²⁴ which allows for detailed interactive processing of the images and fitting of the X-ray absorption spectra contained in the image stacks. More details of STXM measurement and data analysis can be found elsewhere.¹⁹

XANES and XEOL measurements were carried out at the variable line spacing plane grating monochromator (VLS PGM), high resolution spherical grating monochromator (SGM) and soft X-ray microcharacterization (SXRMB) beamlines at CLS. The samples were mounted on conventional carbon tape attached on sample holder with an angle of 45° facing toward the photon beam. XANES were recorded in total electron yield (TEY), fluorescence yield (FLY), and photoluminescence yield (PLY). The TEY was detected with the specimen current and the FLY was measured by detecting the X-ray fluorescence photons from the element of interest using the Si drift detector. TEY is surface-sensitive, while FLY bulk-sensitive. PLY was measured by detecting the optical photons emitted from the sample, which can be recorded in total (zero-order) and partial (wavelength-selective) mode. XEOL spectra were collected using a

dispersive optical spectrometer (200-960 nm, QE65000, Ocean Optics). All XANES and XEOL spectra were normalized to the incident photon flux collected on a refreshed Au grid. More details of XANES and XEOL measurement can be found elsewhere.²³

Results and Discussion

Figure 1a and b show the SEM images of ZnO NW arrays before and after CdS coating. The pure ZnO NWs were grown vertically on the Si substrate with a diameter in the range of 90-200 nm and a length of several micrometers. After CdS coating, the overall wire morphology was maintained and the average diameter increased to about 250-400 nm (Figure 1b and c). The surface of the NWs became very rough. Figure 1d and e show typical TEM images of a single ZnO NW before and after CdS coating, respectively. It is clearly seen that lots of nanoparticles were deposited on the surface of ZnO NW and formed a thick layer showing very irregular surface. The XRD pattern of ZnO NW arrays after CdS coating (Figure 1f) shows two sets of diffraction peaks that correspond to hexagonal ZnO and CdS structures, with no other phases present. The peaks labeled with “*” come from Si and Au, which are the substrate and catalyst used for the synthesis of ZnO NW arrays, respectively. SEM, TEM and XRD results indicate that a layer of CdS nanoparticles was deposited on the surface of ZnO NWs forming ZnO/CdS core/shell NWs albeit an irregular shell.

Detailed characterization of the morphology and chemical composition of the ZnO/CdS nano-composites was carried out by STXM. Figure 2a shows a STXM transmission image of the ZnO/CdS NWs recorded at the O K-edge ($E = 537.2$ eV). The thick NW with high contrast in the middle has a length of 2.2 μm and a diameter of 170-280 nm, which shows the same morphology as those in the SEM and TEM images (Figure 1c and e). A thin and curved NW with low contrast is also shown in the STXM image (located at the bottom right corner of Figure 2a), which has a length of 1 μm and a diameter of about 100 nm.

Zn $L_{3,2}$ -edge, O K-edge and S $L_{3,2}$ -edge XANES spectra collected from the regions of interest (ROIs) marked in the STXM optical density image (Figure 2b) by averaging all stack images at the Zn $L_{3,2}$ -edge, O K-edge and S $L_{3,2}$ -edge are shown in Figure 2c, e and f, respectively. Let us first look at the Zn $L_{3,2}$ -edge XANES spectra in Figure 2c. For the thick NW, the spectra extracted from the trunk (*ROI-3*) and the right-hand side surface (*ROI-2*) show the features of ZnO that correspond to Zn $2p \rightarrow 4s/d$ transitions; and those collected from the left-hand side surface (*ROI-1*), the large particle on the right-hand side surface (*ROI-4*) and the short NW at the bottom (*ROI-5*) display very weak Zn signal but have different features (especially for *ROI-1*). For the thin NW (*ROI-6*), almost no Zn signal was found indicating that it may be CdS.

Normalized Zn $L_{3,2}$ -edge XANES spectra from the ROIs in the thick nanowire are compared with that of hexagonal ZnO and ZnS (Figure 2d). It should be noted that the XANES has the unique ability to distinguish the Zn signal between ZnO (purple curve in Figure 2d) and ZnS (orange curve in Figure 2d) due to its chemical sensitivity to local environments. The normalized spectra from *ROI-2* and *ROI-3* have the same features as that of ZnO. The main features (1021-1028 eV) in the spectrum from *ROI-2* are broadened and less featured, indicating that the surface of ZnO NW becomes more disordered due to the deposition of CdS (large lattice mismatch between ZnO and CdS). Besides the features from ZnO, however, the normalized spectrum from *ROI-1* shows an intense feature at 1023.5 eV (marked by the vertical short dotted line) that agrees well with the main peak in ZnS. It thus indicates that ZnS is present in the near surface region of the ZnO/CdS nano-composites. During the CdS coating, some CdS powders decomposed into Cd and S vapor at high temperature, and the surface region of ZnO NWs could conceivably be firstly sulfurized to ZnS that results in the formation of a ZnS layer (the interface) between ZnO (the core) and CdS (the shell). Therefore, intense feature of ZnS is found in the near surface region (*ROI-1*) of the ZnO/CdS NW. Weak ZnS feature at 1023.5 eV is also observed in the spectrum isolated from *ROI-5*.

Now let us move to O K-edge. The spectrum isolated from the trunk of the thick NW (*ROI-3*) shows characteristic features of ZnO that correspond to O $1s \rightarrow 2p$ transitions, while those from the surface region (*ROI-1* and *ROI-2*) have relatively weak features of ZnO. It indicates that the core of the thick NW is ZnO. The spectra collected from the large particle on the surface (*ROI-4*), the short NW (*ROI-5*) and the thin NW (*ROI-6*) show very weak O signal and exhibit only a broad peak at 537.5 eV without ZnO signature. In previous studies, weak O signal was often found in the O K-edge XANES spectrum of the ZnS nanostructures, which indicates that the surface of ZnS nanostructures was oxidized slightly during their synthesis and storage.²⁵ Therefore, with the absence of intense O signal, we propose that the thin NW (*ROI-6*) and the surface of the thick NW are most likely CdS as the images indicate.

The S $L_{3,2}$ -edge XANES spectra of the ROIs labeled in Figure 2b are shown in Figure 2f. All the spectra except for that from *ROI-1* show exactly the same features as that of CdS. It confirms that the thin NW and the surface of the thick NW are both CdS. However, the spectrum collected from *ROI-1* shows three additional features “a”, “b” and “c” that are from ZnS. Thus ZnS signal was detected in the XANES of the thick NW surface (*ROI-1*) at both Zn and S $L_{3,2}$ -edge, confirming that ZnS was formed on the surface of ZnO NWs during the deposition of CdS. Combining Zn $L_{3,2}$ -edge and O K-edge XANES results, we can conclude that the thick NW in Figure 2a and b is ZnO/CdS core/shell structure with ZnS as interface while the thin NW (*ROI-6*) and the protruding particle (*ROI-4*) are CdS.

STXM chemical maps of the ZnO/CdS nano-composites are displayed in Figure 2g-j. The maps of O (Figure 2i) and S (Figure 2j) clearly illustrate that the core and shell of the nano-composites are ZnO and CdS, respectively. Since STXM can distinguish the Zn signal between ZnO and ZnS,¹⁹ the chemical maps of Zn in the core/shell NW are obtained and shown in Figure 2g and h for the distribution of ZnO and ZnS, respectively. It is interesting to note that ZnS exists in some surface areas of the ZnO NW, acting as the interface (buffer layer) between ZnO (the core) and CdS (the shell) that decreases the lattice mismatch between ZnO and CdS

and reduces the strain in CdS. Due to the fast growth rate of CdS and large lattice mismatch between ZnO (ZnS) and CdS, CdS nanoparticles were grown disorderly on the surface of ZnO NWs (Volmer-Weber growth mode).

ZnO, CdS and ZnS are all important luminescent materials; therefore it is interesting to study the optical properties of the as-prepared ZnO/CdS core/shell NW arrays, especially the origin of the luminescence in such ternary nanostructures. Figure 3 displays the XEOL spectra of the ZnO NW arrays before and after CdS coating excited at different absorption edges. At Zn $L_{3,2}$ -edge ($E_{ex} = 1025$ eV), the spectrum of the ZnO NW arrays before CdS coating (Figure 3a) shows one sharp UV peak at 375 nm and one broad green peak at 500 nm, which are attributed to the near BGE and DE (oxygen/zinc vacancies in the near surface region) of ZnO, respectively. The green emission can be fitted into two Gaussian peaks at 490 and 534 nm, respectively. However, the spectrum of the ZnO NW arrays after CdS coating (Figure 3b) changes dramatically. Several features are noted. First, the intensity of the UV peak (the BGE of ZnO) is almost entirely quenched. It is due to (i) the attenuation length of the incident photon flux by CdS (at 1025 eV, the attenuation length is ~ 200 nm for both CdS and ZnO.) and (ii) defects created on the surface of ZnO NWs during the deposition of CdS, resulting in favor of energy transfer in ZnO NWs from BGE to the competing DE channel. Similar phenomenon was observed in ZnS/ZnO nano-composites that the BGE of ZnS nanobelts was quenched after the deposition of ZnO.¹² Second, the green emission is red shifted and becomes shaper compared to that from pure ZnO NWs. Third, two new broad peaks are observed at the IR region (750 and 900 nm). The Zn $L_{3,2}$ -edge XEOL spectrum (in the region of 400-1000 nm) of the ZnO/CdS NW arrays can be fitted using four Gaussian peaks, located at 511, 537, 750 and 915 nm. The sharp Gaussian peak at 511 nm is the near BGE from CdS ($E_g = 2.42$ eV). While the origin of the other three broad Gaussian peaks at 537, 750 and 915 nm is more complicated since ZnO (the core), CdS (the shell) and ZnS (interface) in the ZnO/CdS nano-composites can all contribute to the green and IR luminescence – (i) both the oxygen/zinc vacancies in ZnO and the sulfur species in ZnS can lead to the green luminescence at 537 nm;^{6-8, 26, 27} and (ii) the defect states (surface/bulk defects) in

ZnO, CdS and ZnS can create IR luminescence.^{7, 9, 10, 28, 29} PL spectrum of the ZnO NW arrays before and after CdS coating is shown in Figure S1. XEOL and PL spectra show the similar features.

It should be noted that the complementary nature of the XANES and XEOL techniques which give site, element and chemical specific measurements allows a better understanding of the interplay and role of each element in the system, especially with soft X-ray excitation. Let us first compare the XEOL spectra of the ZnO/CdS core/shell NW arrays excited at different absorption edges. The O K-edge (Figure 3c) and Cd M_{5,4}-edge (Figure 3d) XEOL spectra are identical to the Zn L_{3,2}-edge spectrum, showing intense green emission and weak IR emission. However, S L_{3,2}-edge (Figure 3e) and S K-edge (Figure 3f) XEOL spectra show weak green emission and strong IR emission. The intensity ratio (peak height ratio) between IR and green emissions of the ZnO/CdS NW arrays is 5 times larger at S L_{3,2}-edge than Zn L_{3,2}-edge. It indicates that the IR luminescence from the ZnO/CdS NW arrays is related to S site in CdS, although ZnS may also contribute.

Now, it is desirable to track the XANES with partial PLY (focused on a particular emission band) as well as total PLY (zero order) to enhance the site specificity (PLY is also known as XEOL yield). Figure 4a displays Zn L_{3,2}-edge XANES spectra of the ZnO/CdS NW arrays. The spectra of standard ZnO and ZnS are shown as reference. The bulk-sensitive FLY spectrum is identical to that of ZnO, while the surface-sensitive TEY spectrum exhibits the features of ZnS. It confirms that ZnS was formed on the surface of ZnO NWs during the deposition of CdS, which is consistent with the STXM results (Figure 2d and h). Let us look at the PLY XANES of the ZnO/CdS NW arrays collected at zero order (250-1000 nm), the UV emission (375 nm), the green emission (511 and 537 nm), and the IR emission (750 and 915 nm). The total PLY and the partial PLY recorded at UV and green region mimic the FLY XANES (only showing ZnO features), illustrating that the UV and green luminescence are related to ZnO. Interestingly, the partial PLY XANES spectra recorded at IR region track neither FLY nor TEY, and remain

constant across the Zn $L_{3,2}$ -edge. It indicates that the Zn site (either ZnO or ZnS) in ZnO/CdS NWs contributes little to the IR luminescence. ZnS does not contribute noticeably to the optical decay since no ZnS signal was found in the PLY XANES.

Figure 4b shows the O K-edge XANES spectra of the ZnO/CdS NW arrays. TEY and FLY show characteristic features of ZnO, which comes from the ZnO core. The total PLY is similar to the TEY and FLY but exhibiting a significant reduction in the feature at 537.2 eV that arises from the excitation of an O $1s$ electron to $2p_{x+y}$ orbitals. It is interesting to compare the partial PLY collected at different wavelength regions. 1) The partial PLY of the UV emission tracks the FLY although the signal is noisy due to the very weak UV luminescence. 2) The partial PLY of the green emission is same to the total PLY; there is a decrease of the feature at 537.2 eV relative to that at 533.8 eV. The above observation agrees well with our previous studies that the partial PLY of the BGE from ZnO nanostructures always mimics their FLY, but that of the DE (surface defects) exhibits a reduction in the feature at 537.2 eV (transition to $2p_z$, the excited state reached following O $1s$ excitation does not couple strongly with the surface defects).³⁰ It confirms that ZnO contributes to the UV and green luminescence from the ZnO/CdS NW arrays. 3) The partial PLY of the IR emission are inverted (negative edge jump) and look different from that of the UV and green emission. They are similar to the O K-edge XANES spectra isolated from the CdS component (e.g.: *ROI-4* and *ROI-6* in Figure 2e). Combining this observation with the partial PLY of the IR emission at Zn $L_{3,2}$ -edge, which indicates that ZnO contributes little to the IR luminescence from the ZnO/CdS NW arrays. We can conclude that CdS is the origin of the IR luminescence.

Figure 4c shows Cd $M_{5,4}$ -edge XANES spectra of the ZnO/CdS NW arrays. TEY and FLY show the features of CdS, which comes from the CdS shell. The total PLY is similar to the TEY and FLY, but is inverted. The partial PLY collected at different regions give additional information about the luminescence from the CdS component. The partial PLY of the UV emission does not track the FLY and TEY, and remains almost constant across the Cd $M_{5,4}$ -edge,

which indicates that the Cd site in the ZnO/CdS NWs contributes little to the UV luminescence that comes from the BGE of ZnO. The partial PLY of the green emission exhibit the features of CdS, but inverted. Normally, the inversion of PLY is due to that the energy transfer from the absorption to the optical channel is less efficient when the edge turns on, or the thickness effect when the X-ray attenuation length is shorter than the sample size. Here we believe the second one is true. The green luminescence at 511 nm (Figure 3d) is from the BGE of CdS and is related to the bulk feature of CdS. The thickness of the CdS shell is estimated to be around 150 nm according to the SEM and TEM images. The X-ray attenuation length is 140 and 60 nm below and at the Cd $M_{5,4}$ -edge, respectively. Therefore, more CdS were excited by incident X-ray beam below the edge than above the edge, leading to the inversion of the partial PLY of the green emission. The partial PLY of the IR emission do not exhibit noticeable Cd signal due to relatively weak IR luminescence and small cross-section at Cd $M_{5,4}$ -edge.

Figure 4d displays S $L_{3,2}$ -edge XANES spectra of the ZnO/CdS NW arrays. TEY, FLY and PLY (zero order) show characteristic features of CdS from the CdS shell. The partial PLY of the green and IR emissions are similar to the TEY and FLY, but inverted due to the thickness effect as described above. The inversion of the partial PLY of the IR emission indicates that the IR luminescence is also related to the bulk feature of CdS and is proposed to be from the bulk defects in CdS. The S K-edge XANES of the ZnO/CdS NW arrays is shown in Figure S2. TEY, FLY and PLY (zero order) are identical to that of CdS.³¹ The S K-edge PLY exhibits positive edge jump, indicating that the energy transfer from S absorption to the optical channel is efficient (thickness effect does not work any more since the X-ray attenuation length is 1 μm at S K-edge). No ZnS signal was observed in the PLY XANES at both S $L_{3,2}$ -edge and K-edge, illustrating that ZnS does not contribute noticeably to the luminescence of the ZnO/CdS NW arrays.

Based on the above XEOL and XANES results and analysis, we arrive at the following for the ZnO/CdS NW arrays: 1) the UV emission (375 nm) comes from the BGE of ZnO; 2) the green

emission are from both the BGE of CdS (511 nm, narrow) and DE of ZnO (537 nm, broad); 3) the IR emission (750 and 915 nm) comes from the DE (bulk defects related to S site) of CdS; 4) ZnS does not contribute noticeably to the luminescence; 5) Compared with ZnO NWs, the BGE and high-energy DE (the Gaussian peak at 490 nm in Figure 3a, which is supposed to come from oxygen vacancies) from ZnO component in the ZnO/CdS nano-composites are almost totally quenched, while the low-energy DE (the Gaussian peak at 534 nm in Figure 3a, which is supposed to be from zinc vacancies) changes little.

CONCLUSION

We have reported the synthesis and characterization of the ZnO/CdS core/shell NW arrays, and investigated the origin of their luminescence via synchrotron-based techniques such as STXM, XANES and XEOL. We have shown that the combined use of XANES and XEOL techniques provides unique capabilities (site, element and chemical specific) to investigate light emitting nanomaterials, especially nano-composites with multiple-component (the presence of ZnS interface in the ZnO/CdS core/shell structure and their luminescence properties in this case). These techniques should be applicable to the characterization of a wide variety of light emitting materials.

Acknowledgements.

We would like to thank beamline scientists T. Regier, L. Zuin and Y. F. Hu for their technical support at CLS, and appreciate Dr. Lyudmila Goncharova and Ms. Carolyn Cadogan for their kind help in PL measurements. Research at the University of Western Ontario is supported by NSERC, CFI, OIT, OMRI and CRC (TKS). CLS is supported by CFI, NSERC, CHIR, NRC, and the University of Saskatchewan. Research at Nanjing University is supported by NNSFC (No. 61176087).

Supporting Information Available: PL spectra of the ZnO NW arrays before/after CdS

coating. S K-edge XANES spectra of the ZnO/CdS core/shell NW arrays. See

DOI: 10.1039/b000000x/.

FIGURES

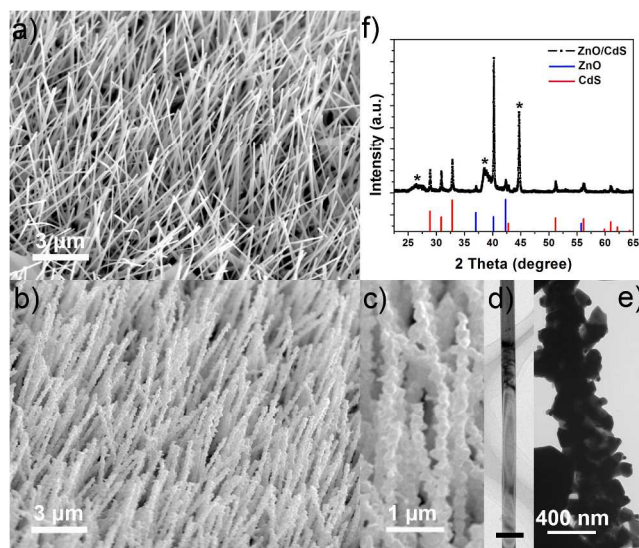


Figure 1. a-b) SEM images of ZnO NW arrays before and after CdS coating, respectively. c) High-magnification SEM image of ZnO NW arrays after CdS coating. d-e) TEM images of a single ZnO NW before and after CdS coating, respectively. Scale bar in d) is 200 nm. f) XRD pattern of the as-prepared ZnO/CdS nano-composites, hexagonal ZnO (JCPDS 80-0075) and hexagonal CdS (JCPDS 77-2306).

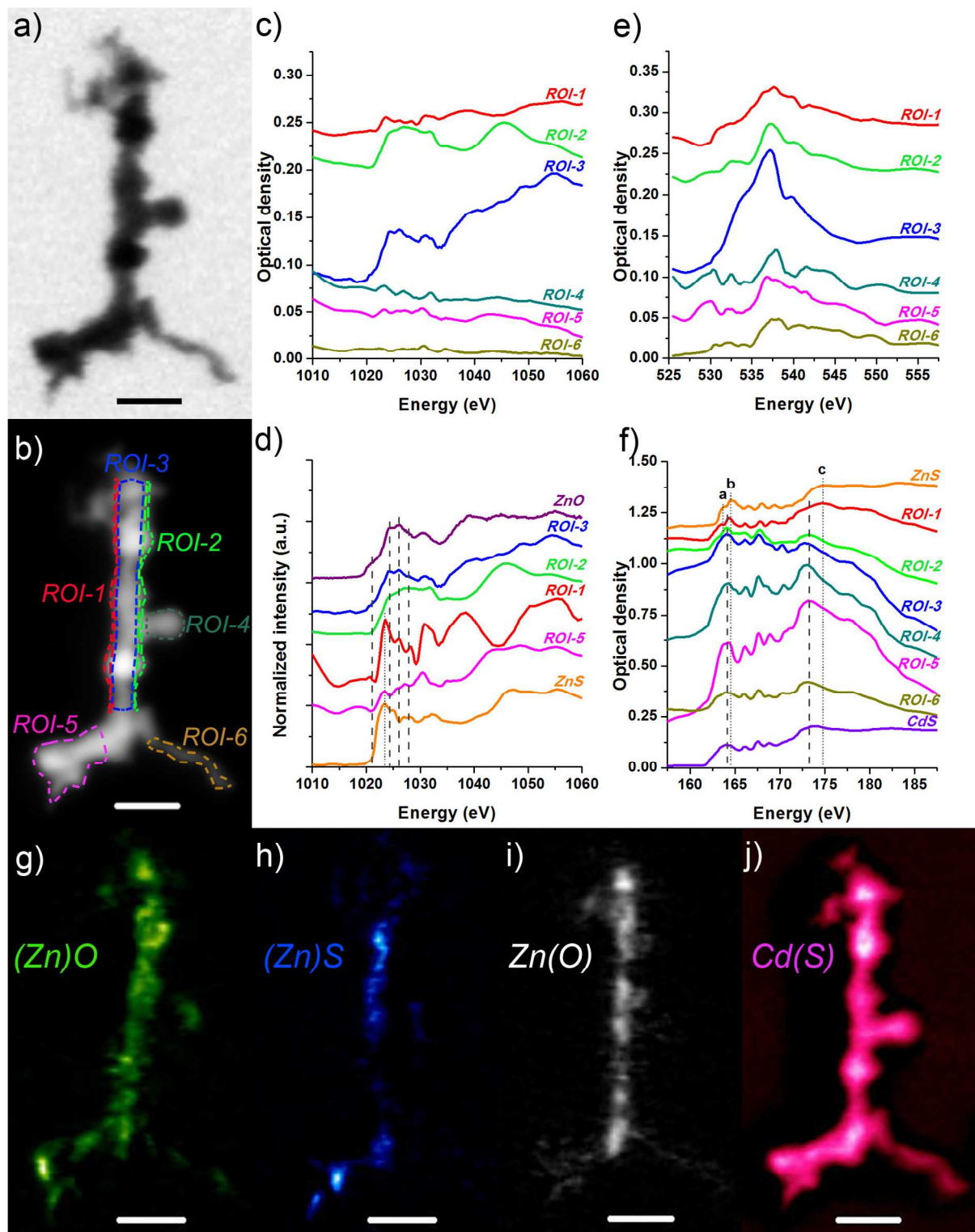


Figure 2. a) STXM transmission image of the ZnO/CdS NWs at 537.2 eV. b) STXM optical density image of the ZnO/CdS NWs (the image was averaged from all stack images at the $S L_{3,2}$ -edge, O K-edge and Zn $L_{3,2}$ -edge). The enclosed color dashed lines indicate the regions of

interest (ROIs) on the ZnO/CdS NWs for extracting XANES spectra. c-f) XANES spectra extracted from the ROIs shown in b) at c) Zn L_{3,2}-edge, e) O K-edge, and f) S L_{3,2}-edge. d) Normalized Zn L_{3,2}-edge XANES spectra from the selected ROIs in b). g-j) STXM chemical maps of g-h) Zn in ZnO and ZnS, respectively), i) O and j) S in the ZnO/CdS NWs. The scale bars in a), b) and g-j) are 500 nm.

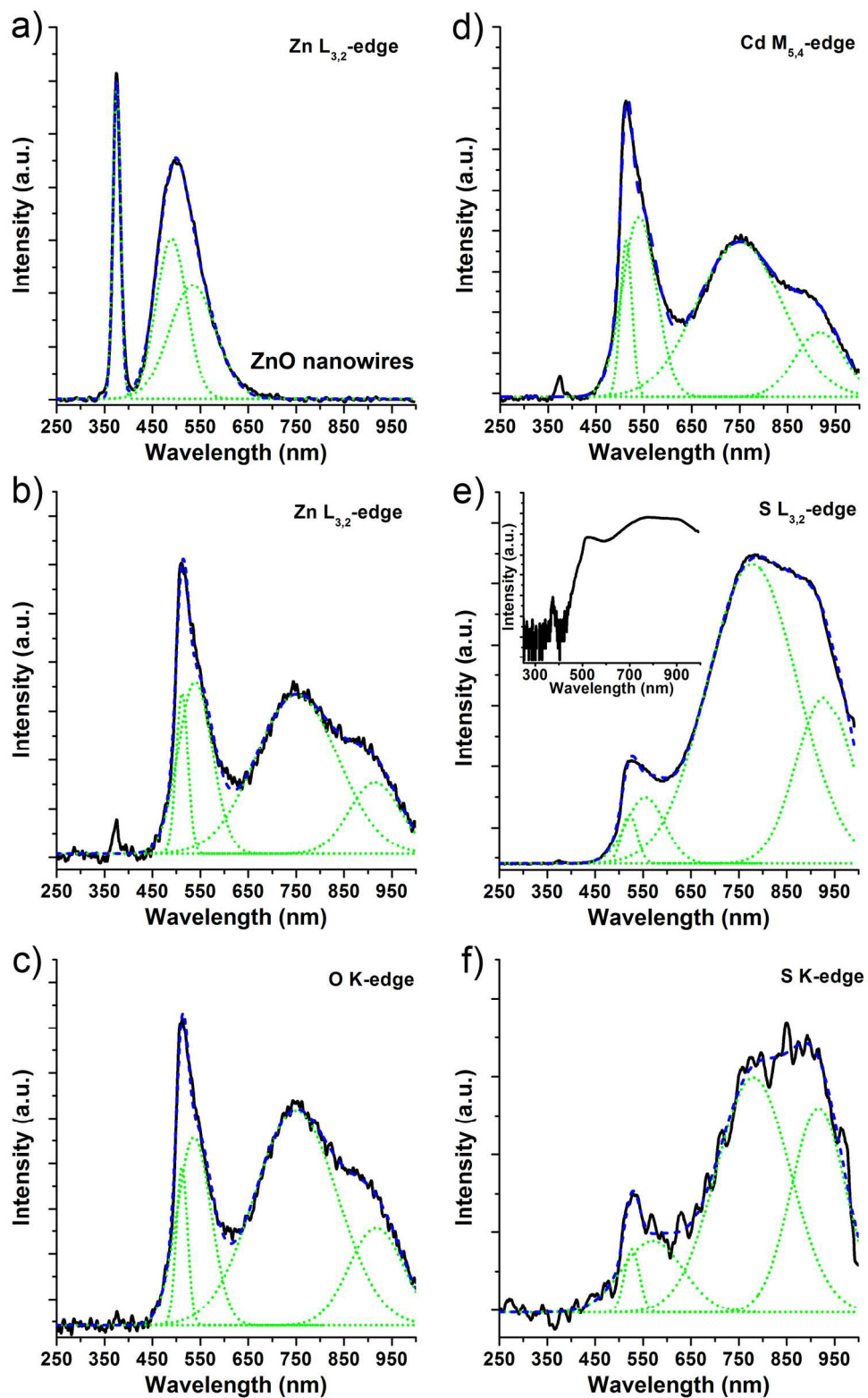


Figure 3. a) XEOL spectrum of the ZnO NW arrays excited at Zn $L_{3,2}$ -edge ($E_{ex} = 1025$ eV). b-f) XEOL spectra of the ZnO/CdS core/shell NW arrays excited at b) Zn $L_{3,2}$ -edge ($E_{ex} = 1025$ eV),

c) O K-edge ($E_{ex} = 535$ eV), d) Cd $M_{5,4}$ -edge ($E_{ex} = 408$ eV), e) S $L_{3,2}$ -edge ($E_{ex} = 164$ eV), and f) S K-edge ($E_{ex} = 2474$ eV). The solid, dashed and dotted curves are raw XEOL, Gaussian fitted XEOL and fitted Gaussian peaks, respectively. The inset of e) is the log scale plot of e).

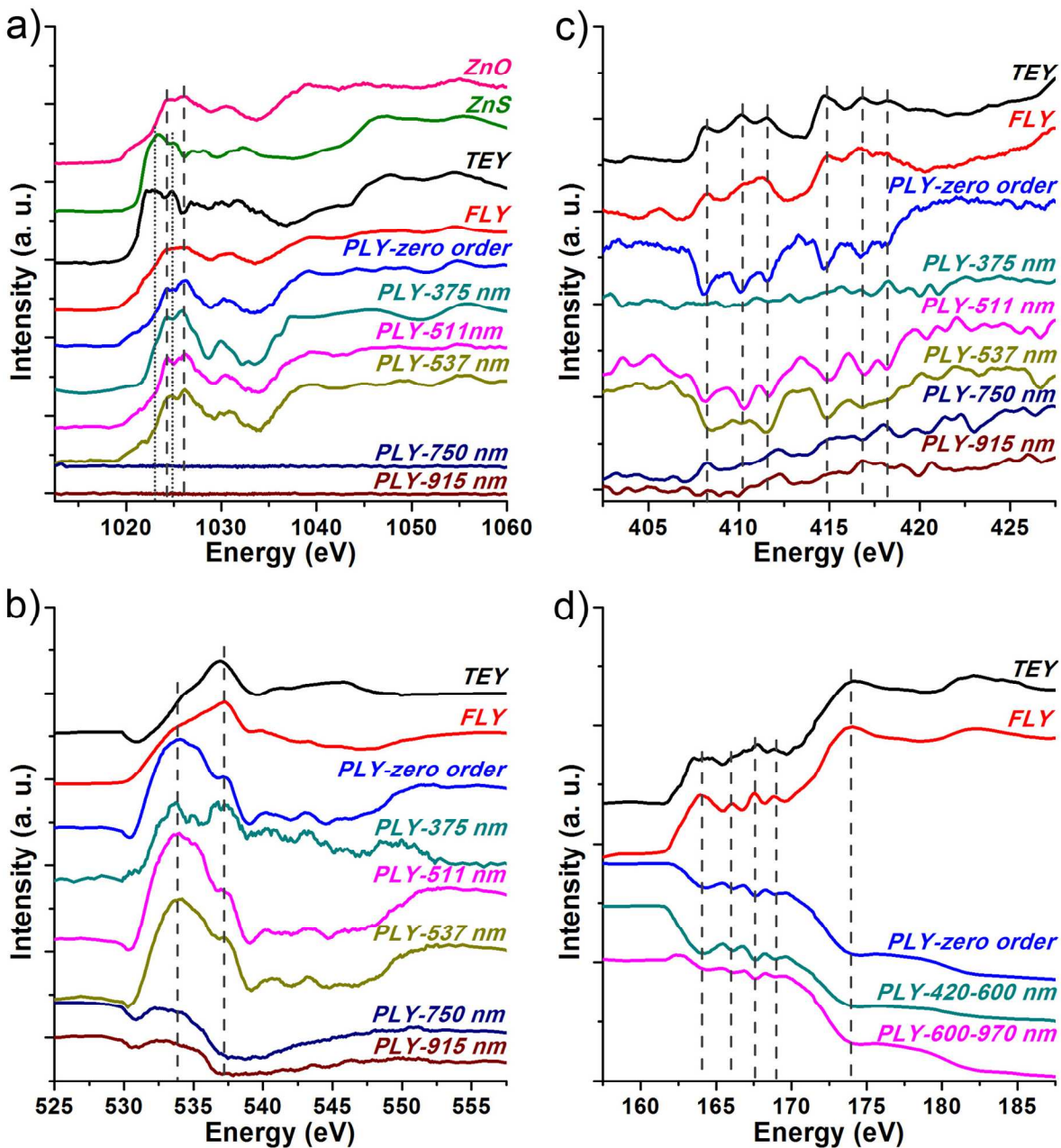


Figure 4. XANES spectra of the ZnO/CdS core/shell NW arrays at a) Zn $L_{3,2}$ -edge, b) O K-edge, c) Cd $M_{5,4}$ -edge, and d) S $L_{3,2}$ -edge. Zn $L_{3,2}$ -edge XANES of hexagonal ZnO and ZnS are also shown in a) for comparison. PLY spectra were recorded in total PLY (zero order) and wavelength-selected PLY.

REFERENCES AND NOTES

1. C. Burda, X. B. Chen, R. Narayanan and M. A. El-Sayed, *Chem Rev*, 2005, **105**, 1025-1102.
2. R. A. Rosenberg, G. K. Shenoy, M. F. Chisholm, L. C. Tien, D. Norton and S. Pearton, *Nano Lett*, 2007, **7**, 1521-1525.
3. X. D. Wang, J. H. Song and Z. L. Wang, *J Mater Chem*, 2007, **17**, 711-720.
4. Z. L. Wang, *Mat Sci Eng R*, 2009, **64**, 33-71.
5. T. Y. Zhai, X. S. Fang, L. Li, Y. Bando and D. Golberg, *Nanoscale*, 2010, **2**, 168-187.
6. U. Ozgur, Y. I. Alivov, C. Liu, A. Teke, M. A. Reshchikov, S. Dogan, V. Avrutin, S. J. Cho and H. Morkoc, *J Appl Phys*, 2005, **98**, 041301.
7. M. S. Wang, Y. J. Zhou, Y. P. Zhang, E. J. Kim, S. H. Hahn and S. G. Seong, *Appl Phys Lett*, 2012, **100**, 101906.
8. J. Smith, A. Akbari-Sharbaz, M. J. Ward, M. W. Murphy, G. Fanchini and T. K. Sham, *J Appl Phys*, 2013, **113**, 093104.
9. G. E. Davidyuk, N. S. Bogdanyuk, A. P. Shavaroova and A. A. Fedonyuk, *Semiconductors*, 1997, **31**, 866-868.
10. Z. Q. Wang, J. F. Gong, J. H. Duan, H. B. Huang, S. G. Yang, X. N. Zhao, R. Zhang and Y. W. Du, *Appl Phys Lett*, 2006, **89**, 033102.
11. M. W. Murphy, X. T. Zhou, J. Y. P. Ko, J. G. Zhou, F. Heigl and T. K. Sham, *J Chem Phys*, 2009, **130**, 084707.
12. Z. Q. Wang, Z. Liu, J. F. Gong, S. Wang and S. G. Yang, *Crystengcomm*, 2011, **13**, 6774-6779.
13. E. D. Spoeke, M. T. Lloyd, Y. J. Lee, T. N. Lambert, B. B. McKenzie, Y. B. Jiang, D. C. Olson, T. L. Sounart, J. W. P. Hsu and J. A. Voigt, *J Phys Chem C*, 2009, **113**, 16329-16336.
14. E. D. Spoeke, M. T. Lloyd, E. M. McCready, D. C. Olson, Y. J. Lee and J. W. P. Hsu, *Appl Phys Lett*, 2009, **95**, 213506.
15. M. Seol, H. Kim, Y. Tak and K. Yong, *Chem Commun*, 2010, **46**, 5521-5523.
16. T. K. Sham, D. T. Jiang, I. Coulthard, J. W. Lorimer, X. H. Feng, K. H. Tan, S. P. Frigo, R. A. Rosenberg, D. C. Houghton and B. Bryskiewicz, *Nature*, 1993, **363**, 331-334.
17. L. J. Liu and T. K. Sham, *Small*, 2012, **8**, 2371-2380.
18. Z. Q. Wang, C. L. Li, L. J. Liu and T. K. Sham, *J Chem Phys*, 2013, **138**, 084706.
19. Z. Q. Wang, J. Wang, T. K. Sham and S. G. Yang, *J Phys Chem C*, 2012, **116**, 10375-10381.
20. L. J. Liu, T. K. Sham, W. Q. Han, C. Y. Zhi and Y. Bando, *Acs Nano*, 2011, **5**, 631-639.
21. M. J. Ward, W. Q. Han and T. K. Sham, *J Phys Chem C*, 2011, **115**, 20507-20514.
22. Z. Q. Wang, J. F. Gong, Y. Su, Y. W. Jiang and S. G. Yang, *Cryst Growth Des*, 2010, **10**, 2455-2459.
23. Z. Q. Wang, X. X. Guo and T. K. Sham, *Nanoscale*, 2014, **6**, 6531-6536.
24. <http://unicorn.mcmaster.ca/aXis2000.html>
25. Unpublished experiments.
26. C. H. Ye, X. S. Fang, G. H. Li and L. D. Zhang, *Appl Phys Lett*, 2004, **85**, 3035-3037.
27. X. S. Fang, C. H. Ye, L. D. Zhang, Y. H. Wang and Y. C. Wu, *Adv Funct Mater*, 2005, **15**, 63-68.

28. C. H. Ye, X. S. Fang, M. Wang and L. D. Zhang, *J Appl Phys*, 2006, **99**, 063504.
29. B. D. Liu, Y. Bando, Z. E. Wang, C. Y. Li, M. Gao, M. Mitome, X. Jiang and D. Golberg, *Cryst Growth Des*, 2010, **10**, 4143-4147.
30. R. A. Rosenberg, G. K. Shenoy, L. C. Tien, D. Norton, S. Pearton, X. H. Sun and T. K. Sham, *Appl Phys Lett*, 2006, **89**, 093118.
31. X. T. Zhou, P. S. G. Kim, T. K. Sham and S. T. Lee, *J Appl Phys*, 2005, **98**, 024312.